# DETERMINATION OF INDOOR DESIGN TEMPERATURE, THERMAL CHARACTERISTICS AND INSULATION THICKNESS UNDER HOT CLIMATE CONDITIONS

**Meral ÖZEL**

Department of Mechanical Engineering, Firat University, 23279 Elazığ, Turkey
mozel@firat.edu.tr, ORCID: 0000-0002-9516-4715

**Abstract:** The base purpose of this work is to use interior design temperatures and the heating and cooling periods, which are determined according to different wall orientations in terms of thermal performance throughout the year, in the calculation of heat transfer characteristics and optimum insulation thickness. This work is realized under dynamic thermal conditions for the climatic conditions of Adana, Turkey. Firstly, the transmission loads for both heating and cooling are determined for uninsulated and insulated walls according to indoor design temperatures: 20, 22, 24 °C. Annual transmission loads, annual average dynamic thermal resistance, annual average time lag, and decrement factor for various wall directions are calculated by using indoor design temperatures determined over the whole year from minimum heating and cooling transmission loads point of view. Then, these loads determined overheating and cooling periods are used for the optimization of insulation thickness. In the uninsulated wall, yearly cooling load is obtained to be 221.37, 152.81, 229.14 and 229.14 MJ/m² for the south, north, east and west orientations, respectively while yearly heating load is obtained to be 73.54, 138.44, 117.62 and 117.62 MJ/m². It is observed that the cooling load is more dominant than the heating load under the climate conditions of Adana. It is also observed that the longest cooling period is obtained in south orientation while the shortest cooling period is obtained in north orientation. The optimum thickness of the insulation for Adana is obtained to be 8.4, 8.0, 9.2 and 9.2 cm for south, north, east and west orientations, respectively. The results indicate that the indoor design temperatures and insulation have a significant effect on heating, cooling and total transmission loads. Besides, the results reveal that the wall orientation has an important effect on heating and cooling periods, dynamic thermal resistance, time lag and optimum insulation thickness.

**Keywords:** Thermal performance, Indoor design temperature, Optimization of insulation thickness, dynamic thermal condition

## SICAK İKLİM ŞARTLARI ALTINDA İÇ DİZAYN SICAKLIĞI, TERMAL ÖZELLİKLER VE YALITIM KALINLIĞININ BELİRLENMESİ

**Özet:** Bu çalışmanın temel amacı, yıl boyunca ısıl performans açısından farklı yönlendirmelere göre belirlenen iç dizayn sıcaklıkları ile ısıtma ve soğutma periyotlarını, ısı transfer karakteristikleri ve optimum yalıtım kalınlığının hesabında kullanmaktır. Bu çalışma, Türkiyenin Adana şehrinin iklim şartları için dinamik termal şartlar altında gerçekleştiriliyor. İlk olarak; 20, 22, 24 °C iç dizayn sıcaklıklarına göre yalıtımsız ve yalıtımlı duvarlar için ısıtma ve soğutma geçiş yükleri belirleniyor. Minimum ısıtma ve soğutma geçiş yükleri açısından bütün yıl üzerinden belirlenen iç dizayn sıcaklıklarını kullanarak değişik duvar yönlendirmeleri için yıllık geçiş yükleri, yıllık ortalama dinamik termal direnç, yıllık ortalama faz kayması ve sönüm oranı belirleniyor. Daha sonra ısıtma ve soğutma periyotları üzerinden belirlenen bu yükler yalıtım kalınlığının optimizasyonu için kullanılıyor. Yalıtımsız duvarda güney, kuzey, doğu ve batı yönleri için yıllık ısıtma yükü sırasıyla 73.54, 138.44, 117.62 ve 117.62 MJ/m² olarak elde edilirken, yıllık soğutma yükü sırasıyla 221.37, 152.81, 229.14 ve 229.14 MJ/m² olarak elde edilmiştir. Adananın iklim şartları altında soğutma yükünün ısıtma yükünden daha baskın olduğu görülüyor. Ayrıca, en kısa soğutma periyodunun kuzeyde elde edildiği, en uzun soğutma periyodunun ise güneyde elde edildiği görülüyor. Adana için optimum yalıtım kalınlığı; güney, kuzey, doğu ve batı yönleri için sırasıyla 8.4, 8.0, 9.2 and 9.2 cm olarak elde edilmiştir. Sonuçlar iç dizayn sıcaklığı ve yalıtımın; ısıtma, soğutma ve toplam geçiş yükleri üzerinde önemli bir etkiye sahip olduğunu gösteriyor. Ayrıca, sonuçlar duvar yönlendirmenin ısıtma ile soğuma periyotları üzerinde ve dinamik termal direnç, faz kayması ve optimum yalıtım kalınlığı üzerinde önemli bir etkiye sahip olduğunu da gösteriyor.

**Anahtar Kelimeler:** Termal performans, İç dizayn sıcaklığı, Yalıtım kalınlığının optimizasyonu, Dinamik termal şart

**NOMENCLATURE**

| | |
|---|---|
| $c$ | specific heat [J/kg K] |
| $C_A$ | total energy consumption cost [\$/m² year] |
| $C_i$ | insulation cost [\$/m³] |
| $C_E$ | electricity cost [\$/kWh] |
| $C_F$ | fuel cost [\$/m³] |
| $COP$ | coefficient of performance |
| $h_i$ | convection heat transfer coefficient at the wall inner surface [W/m² K] |
| $h_o$ | convection heat transfer coefficient at the wall outer surface [W/m² K] |
| $H_u$ | lower heating value of the fuel [J/m³] |
| $I_T$ | total solar radiation for a vertical surface [W/m²] |
| $k$ | thermal conductivity [W/m K] |
| $L_i$ | thickness of insulation [m] |
| $PWF$ | present worth factor |
| $q_i$ | instantaneous heat flux at the wall indoor surface [W/m²] |
| $Q_g$ | heating transmission load [J/m²] |
| $Q_l$ | cooling transmission load [J/m²] |
| $R_n$ | nominal thermal resistance [m².K/W] |
| $R_d$ | dynamic thermal resistance [m².K/W] |
| $t_{T_{es}(max)}$ | time that external surface temperature are being maximum [h] |
| $t_{T_{is}(max)}$ | time that internal surface temperature are being maximum [h] |
| $T_{id}$ | indoor design temperature [ºC] |
| $T_o$ | outdoor environmental temperature [ºC] |
| $T_{sa}$ | sol-air temperature [ºC] |
| $T_{is(max)}$ | maximum internal surface temperature [ºC] |
| $T_{is(min)}$ | minimum internal surface temperature [ºC] |
| $T_{es(max)}$ | maximum external surface temperature [ºC] |
| $T_{es(min)}$ | minimum external surface temperature [ºC] |

*Greek letters*

| | |
|---|---|
| $\alpha$ | wall outdoor surface solar absorptivity |
| $\delta$ | declination angle [deg.] |
| $\phi$ | latitude angle [deg.] |
| $\Phi$ | time lag [h] |
| $f$ | decrement factor |
| $\gamma$ | surface azimuth angle [deg.] |
| $\eta_s$ | heating system efficiency |
| $\rho$ | density [kg/m³] |
| $\omega$ | hour angle [deg.] |
| $\theta$ | incidence angle [deg.] |
| $\theta_z$ | zenith angle [deg.] |

**INTRODUCTION**

Energy consumption which is shared among industrial, transportation, building and agriculture sectors is rising rapidly due to urbanization and population growth (Bolattürk, 2008). The buildings are the biggest energy consumer after the industrial sector and create 40% of the energy consumption. Building envelope plays a major role in maintaining indoor comfort conditions under varying outdoor climatic conditions (Zenginis and Kontoleon, 2017; Kontoleon et al., 2013)

The outer envelope that forms the buildings interacts continuously with the changing ambient temperature and solar radiation. In consequence of this interaction, the outer surface temperature of the building envelope and the heat conduction through the wall change continuously depending on the time. This change affects the interior environment considerably. As known, a large amount of the energy consumed in buildings is employed for heating and cooling of buildings to provide internal comfort. Therefore, heating and cooling loads in buildings constitute a significant part of the energy consumption of the buildings. One of the most effective ways to decrease these loads is to use heat insulation in the building envelope. Thermal resistance is increased by using heat insulation on building exterior walls while heat transfer loads are reduced. On the other hand, proper utilization of thermal insulation improves thermal properties such as time lag and decrement factor that expresses the thermal storage capacity of the outer walls. That is, thermal insulation leads to an increase in time lag and reduce in decrement factor. As the insulation thickness applied to the outer walls of buildings rises, the heat transfer reduces, and the insulation cost increases. Therefore, the insulation's optimum thickness should be determined based on a cost analysis.

To estimate the heat transition loads used in the determination of optimization of insulation thickness, many works in the literature applied degree-day or degree-hour method which is a crude and simple model under static conditions (Akan, 2021; Aktemur et al., 2021; Bolattürk, 2008; Dombaycı et al., 2006; Hasan, 1999; Çomaklı and Yüksel, 2003; Sisman et al., 2007; Ozkahraman and Bolattürk, 2006; Çomaklı and Yüksel, 2004; Dombaycı, 2007; Dombaycı et al., 2017; Ertürk, 2016; Ertürk, 2017; Yıldız et al., 2008; Kaynaklı, 2008; Mahlia and Iqbal, 2010; Kurt, 2010; Bolattürk, 2006; Kaynaklı et al., 2015; Yu et al., 2009; Özel et al., 2015; Barrau, 2014; Sundarama and Bhaskaran, 2014). However, a more accurate estimation of heating and cooling transition loads is quite important in the determination of the optimum insulation thickness. Therefore, Dynamic transient models considering the effects of solar radiation and the thermal storage of the building are more reliable for estimating heat loads. In literature, a few studies based on the thermal performance of the building walls used numerical model under dynamic thermal conditions (Al-Sanea et al., 2005; Ozel, 2011; Ozel, 2013a; Ozel, 2013b;

50

Nematchoua et al., 2017; Huo et al., 2015; Ramin et al., 2016; Ibrahim et al., 2012; Al-Sanea et al., 2003; Al-Sanea and Zedan, 2002) while the others applied an analytical dynamic model based on Complex Finite Fourier Transform (CFFT) method (Daouas, 2011; Daouas et al., 2010).

There are several studies in the literature on determining thermal performance and optimum insulation thicknesses considering different wall orientations. In all of these works, the interior design temperatures and the heating and cooling periods which are determined for the representation day of each month are independent of the wall orientations. The basic aim of this work is to fill this knowledge gap and to analyze the wall insulation both thermally and economically considering many parameters such as heating, cooling, and total transmission loads, static and dynamic thermal resistances, time lag, decrement factor, and optimum insulation thickness. Several studies in the literature include only a few of these parameters. In this study, firstly, the interior design temperatures are numerically determined from minimum heat gain and loss point of view by considering wall orientations under dynamic thermal conditions. Secondly, the interior design temperatures which are determined according to wall orientations are used to determine thermal parameters such as annual transmission loads, annual average dynamic thermal resistance, annual average time lag, and decrement factor. The transmission loads are separately calculated as hourly, daily, and yearly. Finally, optimum insulation thickness is also calculated by using heating and cooling periods determined according to wall orientations. The results of this work which is realized for the climate conditions of Adana, Turkey are compared with results of other works under various climate conditions.

## MATHEMATICAL FORMULATION

The uninsulated and insulated composite wall structures are illustrated schematically in Fig.1. The outer side of the walls is exposed to the external environment temperature and solar radiation changing throughout the day while the inner side is exposed to the indoor design temperature at a fixed temperature. One dimensional transient heat conduction equation in a composite wall with perfect thermal contact is defined as:

$$\frac{\partial T_j}{\partial t} = \frac{k_j}{\rho_j c_j} \frac{\partial^2 T_j}{\partial x^2}, \qquad j = 1,2,...,N \tag{1}$$
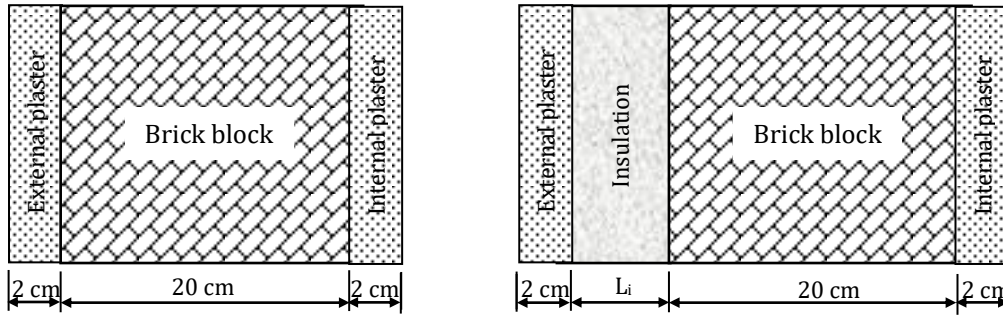


**Figure 1.** Uninsulated and insulated wall structures

Thermal properties used in the composite wall are given in Table 1. It is considered that there is no heat generation, interface resistance is neglected and change of thermal properties is neglected. One initial condition and two boundary conditions are needed to solve the differential equation. An arbitrary homogeneous temperature range is chosen as the initial condition. The convection boundary conditions on the outer and inner surfaces of the wall are described as follows, respectively:

**Table 1.** Material properties

| Material | k (W/m K) | ρ (kg/m³) | c (J/kg K) |
|---|---|---|---|
| Brick block | 0.620 | 1800 | 840 |
| Expanded polystyrene | 0.038 | 18 | 1500 |
| Cement plaster | 0.720 | 1865 | 840 |

$$-k_{EP} \cdot \frac{\partial T(0,t)}{\partial x} = h_0 (T_{sa} - T_{es}) \tag{2}$$

$$-k_{IP} \cdot \frac{\partial T(L,t)}{\partial x} = h_i (T_{is} - T_{id}) \tag{3}$$

where $k_{EP}$ and $k_{IP}$ are thermal conductivities of external and internal plaster, respectively. $h_o$ and $h_i$ are convection heat-transfer coefficients at the wall outer and inner surfaces, respectively. $T_{es}$ and $T_{is}$ are the external and internal surface temperatures of wall, respectively. $T_{id}$ is the internal design temperature. $T_{sa}$ is called as sol-air temperature and is described as follows (Threlkeld, 1998):

$$T_{sa} = T_o + \alpha I_T / h_o - \varepsilon \Delta R / h_o \tag{4}$$

$T_o$ and $\alpha$ are external environment temperature changing throughout the day and outer surface solar absorptivity, respectively. The outdoor environment temperatures are given in Table 1. $\varepsilon \Delta R/h_o$ is called as the correction factor and is taken as 0 for vertical wall surfaces. $I_T$ is the total solar radiation and is calculated for vertical wall surfaces as follows (Duffie and Beckman, 1991):

$$I_T = R_b I_b + (I_d + \rho_g I)/2$$

(5) where $I$, $I_b$ and $I_d$ are total, beam and diffuse solar radiations on the horizontal surface. $\rho_g$ is the reflectance of the ground and is taken as 0.2. $R_b$ is called as the geometric factor and is calculated depending on incidence angle ($\Theta$) and zenith angle ($\Theta_z$) as follows:

$$R_b = \cos\theta / \cos\theta_z \qquad (6)$$

These angles are given for vertical surfaces as follows:

$$\cos\theta = \cos\delta.\sin\varphi.\cos\gamma.\cos\omega$$
$$+\cos\delta.\sin\gamma.\sin\omega$$
$$-\sin\delta.\cos\varphi.\cos\gamma \qquad (7)$$

$$\cos\theta_z = \cos\varphi.\cos\delta.\cos\omega + \sin\varphi.\sin\delta \qquad (8)$$

where $\phi$, $\delta$, $\gamma$ and $\omega$ represent latitude angle, declination angle, surface azimuth angle and hour angle, respectively. The surface azimuth angle is taken to be 0 for a south-facing wall, 180 for a north-facing wall, -90 and 90 for east and west orientations, respectively.

For determining the temperature distribution through the composite structure, the heat conduction equation containing boundary conditions was previously solved by employing the implicit finite-difference method (Ozel and Pihtili, 2007) and a general-purpose computer program was developed in MATLAB. To achieve a stable periodic solution, it is assumed that the solar air temperature which associates the effects of external environment temperature and solar radiation will be repeated on sequent days.

**Environmental Conditions**

This work is realized for the climate conditions of Adana (latitude: 36.98ºN, longitude: 35.33ºE), Turkey. Adana which is placed on Turkey's Mediterranean coast is one of the hottest cities of Turkey. Hourly outdoor environment temperatures are supplied from records for weather data in the meteorological station (2007-2017). These hourly temperatures are obtained by taking the average of the years given and are given in Table 2 for the fifteenth day of each month. The solar radiation on vertical wall surfaces is determined via the isotropic sky model (Duffie and Beckman, 1991). $\alpha$ is accepted as 0.8. $h_o$ and $h_i$ are assumed as 22 and 9 W/m$^2$K, respectively (Ozel, 2013a). Sol-air temperatures are determined depending on the solar radiation intensity and the outdoor air temperatures.

**Table 2.** Hourly outdoor environment temperatures for the fifteenth day of each month during the year

| Time (h) | Jan. | Feb. | Mar. | Apr. | May | Jun. | Jul. | Aug. | Sep. | Oct.. | Nov. | Dec. |
|---|---|---|---|---|---|---|---|---|---|---|---|---|
| | | | | | Hourly outdoor environmental temperatures (ºC) | | | | | | | |
| 1 | 9.7 | 11.8 | 14.3 | 18.0 | 21.5 | 23.1 | 27.3 | 27.9 | 24.0 | 20.8 | 15.9 | 1.5 |
| 2 | 11.1 | 11.9 | 14.8 | 17.5 | 21.6 | 22.2 | 27.0 | 28.1 | 23.6 | 20.3 | 15.8 | 0.6 |
| 3 | 9.7 | 11.8 | 14.3 | 17.2 | 20.6 | 22.8 | 26.8 | 27.9 | 23.6 | 21.0 | 15.6 | -0.6 |
| 4 | 8.9 | 11.5 | 13.5 | 16.9 | 20.4 | 22.7 | 26.6 | 27.9 | 23.4 | 18.6 | 14.9 | 1.4 |
| 5 | 6.6 | 11.2 | 12.8 | 16.4 | 21.1 | 24.3 | 28.8 | 27.6 | 23.4 | 18.6 | 14.9 | 1.4 |
| 6 | 6.4 | 10.8 | 12.5 | 18.0 | 22.9 | 25.0 | 28.1 | 28.5 | 24.6 | 19.8 | 15.6 | 1.8 |
| 7 | 6.2 | 10.7 | 11.9 | 19.0 | 25.3 | 25.5 | 29.7 | 29.3 | 26.1 | 23.0 | 16 3 | 2.9 |
| 8 | 8.7 | 10.4 | 12.6 | 20.4 | 26.6 | 27.1 | 30.7 | 32.0 | 28.3 | 25.3 | 17.2 | 5.4 |
| 9 | 8.1 | 11.6 | 14.9 | 20.6 | 27.9 | 27.1 | 31.8 | 32.7 | 29.4 | 27.0 | 19.0 | 7.4 |
| 10 | 11.3 | 14.0 | 16.4 | 21.0 | 28.2 | 28.6 | 32.4 | 33.7 | 30.7 | 28.9 | 20.8 | 9.2 |
| 11 | 13.1 | 16.8 | 17.7 | 21.1 | 28.1 | 29.8 | 33.6 | 34.5 | 31.4 | 30.0 | 22.4 | 10.6 |
| 12 | 14.4 | 19.2 | 18.6 | 21.8 | 27.8 | 29.7 | 33.6 | 34.7 | 31.5 | 29.6 | 23.5 | 11.0 |
| 13 | 16.1 | 21.4 | 19.7 | 21.7 | 27.8 | 29.3 | 34.3 | 35.0 | 31.2 | 30.6 | 23.4 | 11.6 |
| 14 | 17.0 | 22.1 | 20.2 | 21.6 | 26.6 | 29.6 | 33.4 | 34.8 | 30.6 | 30.3 | 23.4 | 11.0 |
| 15 | 17.2 | 22.0 | 20.9 | 21.6 | 26.2 | 29.7 | 32.6 | 33.4 | 27.2 | 30.0 | 22.3 | 9.8 |
| 16 | 17.6 | 22.3 | 17.5 | 21.2 | 24.0 | 29.2 | 31.6 | 33.0 | 23.5 | 27.2 | 21.4 | 8.2 |
| 17 | 17.1 | 22.0 | 17.5 | 20.3 | 22.9 | 26.7 | 31.0 | 31.3 | 24.0 | 24.7 | 20.2 | 7.6 |
| 18 | 13.6 | 20.5 | 17.2 | 19.2 | 22.4 | 25.6 | 29.5 | 30.2 | 21.2 | 22.7 | 19.8 | 7.2 |
| 19 | 10.3 | 16.7 | 16.2 | 18.7 | 22.3 | 24.5 | 29.0 | 29.5 | 22.0 | 23.5 | 18.9 | 5.5 |
| 20 | 8.9 | 14.8 | 15.0 | 18.4 | 22.2 | 24.2 | 28.5 | 28.7 | 22.3 | 20.0 | 17.2 | 5.1 |
| 21 | 8.8 | 14.8 | 14.6 | 18.3 | 22.0 | 24.0 | 28.3 | 28.6 | 22.2 | 20.1 | 17.1 | 4.4 |
| 22 | 8.5 | 13.4 | 14.3 | 18.5 | 21.5 | 23.6 | 28.3 | 28.2 | 21.4 | 19.6 | 16.3 | 3.3 |
| 23 | 8.2 | 13.2 | 13.7 | 18.4 | 21.2 | 23.6 | 28.3 | 27.8 | 21.2 | 19.1 | 16.5 | 2.1 |
| 24 | 8.1 | 12.7 | 13.1 | 18.3 | 21.2 | 22.9 | 27.9 | 27.5 | 21.2 | 17.3 | 15.8 | 2.5 |

## CALCULATION OF THERMAL PARAMETERS

### Heating, Cooling, and Total Transmission Loads

In this work, the fifteenth day of each month during the year is taken into consideration as a representative day and hourly heat transmission loads are calculated as follows:

$$q_i = h_i(T_{is} - T_{id}) \qquad (9)$$

Daily transmission loads are also calculated by integrating instantaneous load over one day period (24 h) as:

$$Q_{id} = \int_0^{24h} q_i \, dt \qquad (10)$$

To calculate a daily total load, these instantaneous loads are integrated over 24 h periods. The daily value of the representative day of each month is multiplied by the number of days in that month.

Yearly total heating and cooling transmission loads are determined separately from daily heating and cooling loads which are summed up over winter and summer periods.

### Nominal and Dynamic Thermal Resistances

Nominal (static) thermal resistance is calculated by summing the convective and conductive resistances as follows (Al-Sanea et al., 2013):

$$R_n = \sum_{j=1}^{N} (L/k)_j + (1/h_i) + (1/h_o) \qquad (11)$$

The average daily dynamic resistance for each month's fifteenth day is obtained as follows (Al-Sanea et al., 2013):

$$R_d = \frac{\int_0^{24h} |(T_o - T_i)| \, dt}{\int_0^{24h} |q_i| \, dt} \qquad (12)$$

The annual average dynamic resistance is calculated to be the weighted average of monthly values according to transmission loads.

### Time Lag and Decrement Factor

There are two features that are beneficial to express the thermal storage capabilities of the outer walls of the building. These features are named as time lag and decrement factor. The time lag is the time when sinusoidal temperature fluctuation achieves from external surface to internal surface of the wall and is defined as follows (Ozel and Pihtili, 2007):

$$\Phi = t_{T_{es}(\max)} - t_{T_{is}(\max)} \qquad (13)$$

Where $t_{T_{es}(\max)}$ and $t_{T_{is}(\max)}$ symbolize the time that external and internal surface temperatures are being maximum, respectively. The decrement factor is the ratio of the internal surface temperature amplitude to the outer surface temperature amplitude, and is defined as follows (Ozel and Pihtili 2007):

$$f = [T_{is(\max)} - T_{is(\min)}] / [T_{es(\max)} - T_{es(\min)}] \qquad (14)$$

Where $T_{es(\max)}$, $T_{is(\max)}$, $T_{es(\min)}$ and $T_{is(\min)}$ are the highest and the lowest temperatures on the external and internal surfaces of the wall. Values of the time lag and decrement factor are determined for each month's fifteenth day. Then, annual values are calculated by taking the arithmetic average of monthly values throughout the year.

### Optimization of Insulation Thickness

The optimization of the insulation thickness is based on a cost analysis which includes the cost of energy consumption and the cost of insulation over the 20-year life of the building. Only heat transmissions from external walls are taken into account for the calculation of the optimum thickness of the insulation. The annual energy consumption cost is calculated as follows considering both the heating and cooling loads:

$$C_A = \frac{Q_h.C_F}{H_u.\eta_s} + \frac{Q_c.C_E}{3.6 \times 10^6.COP} \qquad (15)$$

where $Q_h$ and $Q_c$ are heating and cooling transmission loads per year of the insulated wall, respectively. $C_F$ and $C_E$ are fuel cost and electricity cost, respectively. $H_u$ is the lower calorific value of the fuel, $\eta_s$ is the heating system efficiency and $COP$ is the performance coefficient. The total cost is determined by adding the insulation cost to the present worth of the energy consumption cost over the lifetime of the building and is defined as follows:

$$C_t = C_A.PWF + C_i.L_i \qquad (16)$$

where $C_i$ and $L_i$ are the insulation cost and thickness. $PWF$ is Present Worth Factor. $PWF$ is determined based on inflation and interest rates over the 20-year life of the building (Ozel, 2013). Table 3 gives parameters used in cost analysis.

**Table 3.** The parameters used in calculations

| Parameter | Value |
|---|---|
| Natural gas (in heating) | |
| $C_F$ | 0.4919 \$/m$^3$ |
| $H_u$ | 34.541*10$^6$ J/m$^3$ |
| $\eta_s$ | % 93 |
| Electricity (in cooling) | |
| $C_E$ | 0.1894 \$/kWh |
| $COP$ | 2.5 |
| Insulation | |
| Expanded polystyrene | |
| $C_i$ | 188.419 \$/m$^3$ |
| PWF | 17.75 |

53

## RESULTS AND DISCUSSION

### Determination of Solar Radiation and Sol-air Temperature

Fig. 2(a-b) presents the maximum of the solar radiation and sol-air temperature according to months for different wall orientations. It is revealed that **the** highest values of maximum solar radiation appear in the south-facing wall for October, November, December, January, February and March months while they appear in east and west orientations for April, May, June, July, August and September. The results show that the highest value of maximum solar radiation for all months is obtained to be 553.88 W/m$^2$ in the east (or west) facing wall while the lowest value of maximum solar radiation is obtained as 98.72 W/m$^2$ in the north-facing wall. It is seen that for all months, the minimum solar radiation constitutes in north-facing wall. It is also seen in Fig. 2b that the highest value of sol-air temperature for all orientations is obtained in August month that maximum outdoor temperature occurs.

The results indicate that the maximum of sol-air temperatures for west orientation is higher compared to the other orientations. It is obvious that this is due to the time at which the highest external temperature occurs.

### Determination of Outdoor and Indoor Surface Temperatures

Fig. 3(a-b) indicates the hourly variation of outside surface temperature for January 15 and July 15, respectively. The conclusions show that on January 15, the highest value of outside surface temperatures is obtained to be 27.26 ºC at 13:00 for the south-facing wall while on July 15, it is obtained to be 46.99 ºC at 16:00 for the west-facing wall. Besides, it is seen that in summer, the time that outdoor surface temperature is maximum is obtained to be 13:00, 13:00, 9:00 and 16:00 for the south, north, east and west orientations, respectively. The conclusions indicate that the highest value of the outer surface temperature is reached at the earliest east wall.



**(a)**



**(b)**

**Figure 2 (a-b).** Maximum values of the incident solar radiation and sol-air temperature according to months for different orientations
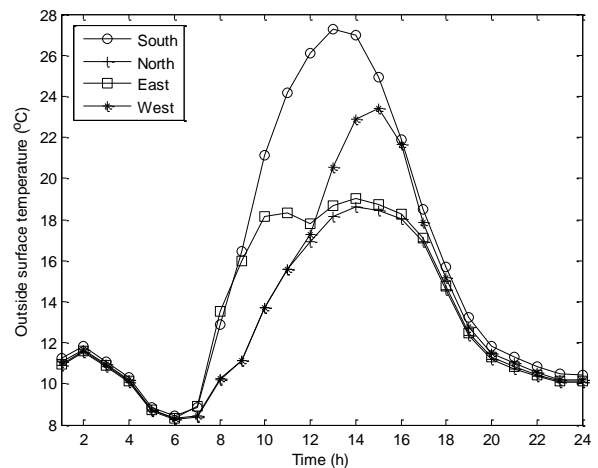


**(a)**
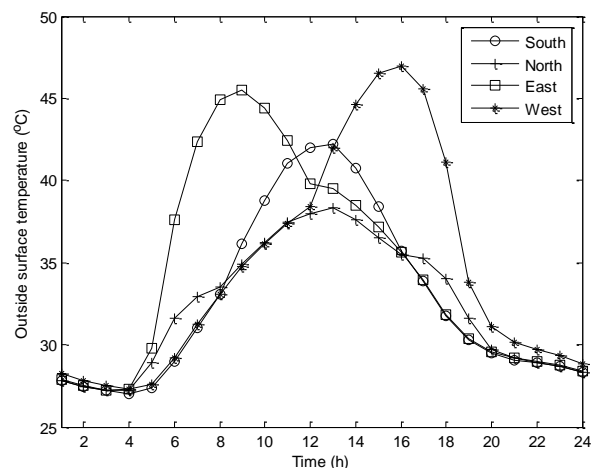


**(b)**

**Figure 3.** Hourly variation of outside surface temperature for a) January 15 and b) July 15

Fig. 4(a-b) presents the hourly change of internal surface temperatures according to wall orientations for

winter and summer conditions, respectively. It is seen that on July 15, maximum values of inside surface

temperatures are obtained to be 26.82, 26.50, 27.24 and 27.55 °C, respectively while on January 15, they are obtained to be 20.02, 18.89, 19.13 and 19.27 °C for south, north, east and west orientations. The results show that for winter, the maximum peak of inside surface temperature achieves in the south-facing wall while for summer, it achieves in the west-facing wall.
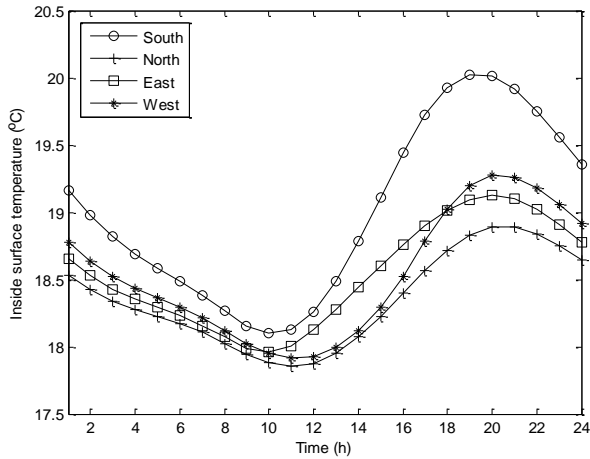


**(a)**
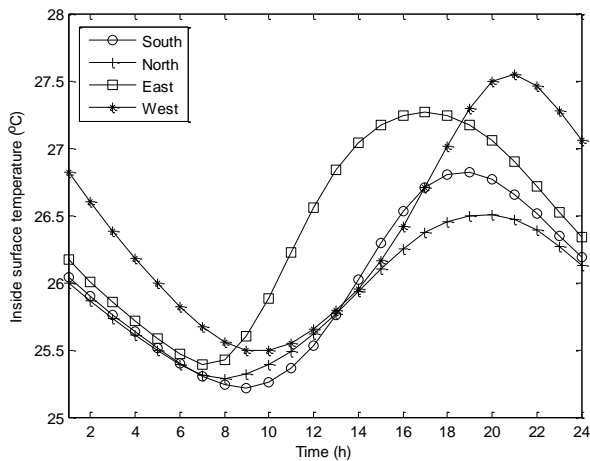


**(b)**

**Figure 4.** Hourly variation of inside surface temperature for a) January 15 and b) July 15

### Determination of Indoor Design Temperatures

Fig. 5 (a-c) indicates daily transmission loads in the uninsulated wall for each month's fifteenth day according to different wall orientations and indoor design temperatures: 20, 22 and 24 °C. These loads for the 6 cm insulated wall are also shown in Fig. 6 (a-c). It is observed that the cooling and heating loads are importantly reduced when the wall is insulated. This reduction is obtained to be 74.7% for all wall orientations and three different indoor design temperatures. In both uninsulated and insulated walls, it is obvious that the highest heating load is reached in December for all orientations while the highest cooling load is reached in August for the south, east and west orientations. But, the highest cooling load for the north-facing wall is obtained in July. The results show that both heating and cooling requests occur in April and

November months according to indoor design temperatures. This indicates that there may be cooling during the day period and heating during the night period.
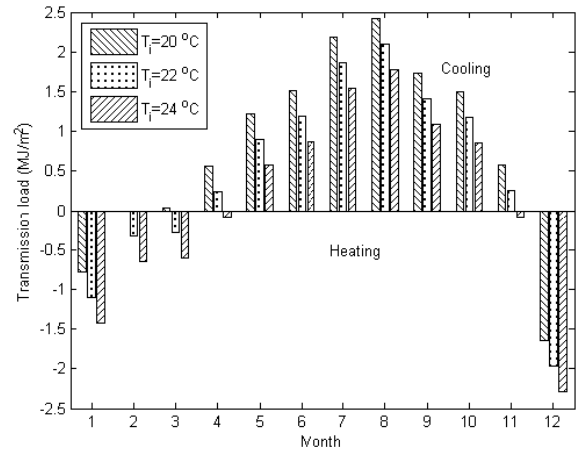


**(a)**
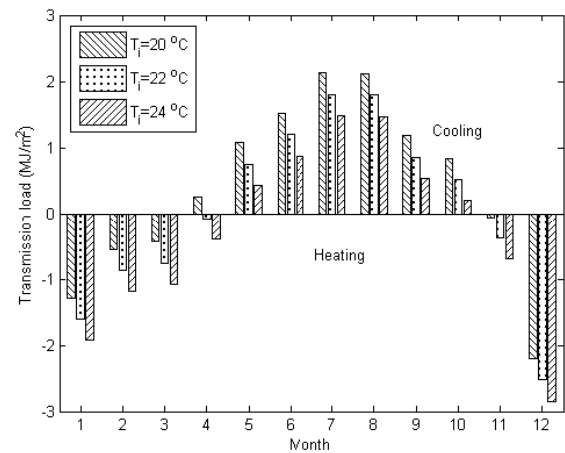


**(b)**
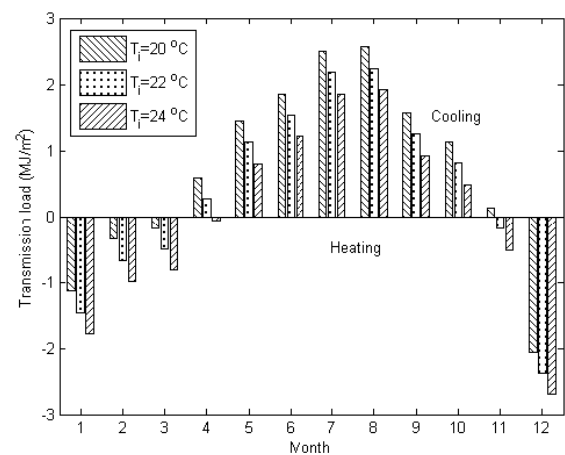


**(c)**

**Figure 5.** The daily total cooling and heating transmission loads for the 15th day of each month with respect to different indoor design temperatures in the uninsulated wall for (a) south, (b) north and (c) east (or west) orientations.
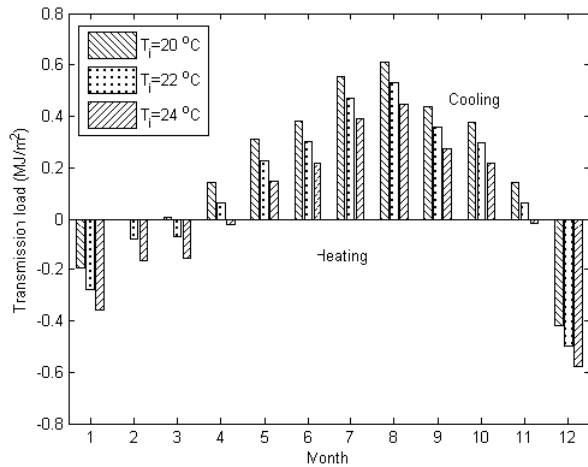
**(a)**
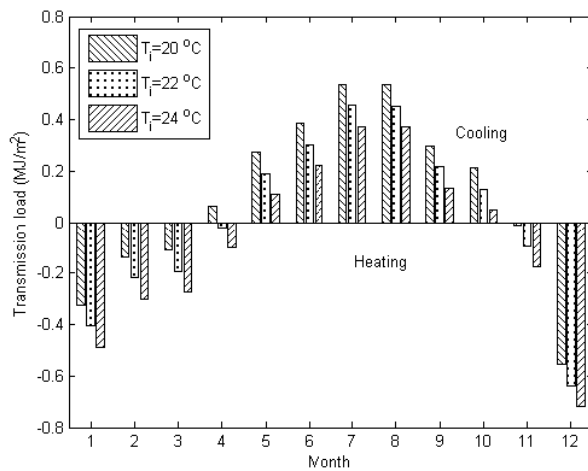


**(b)**
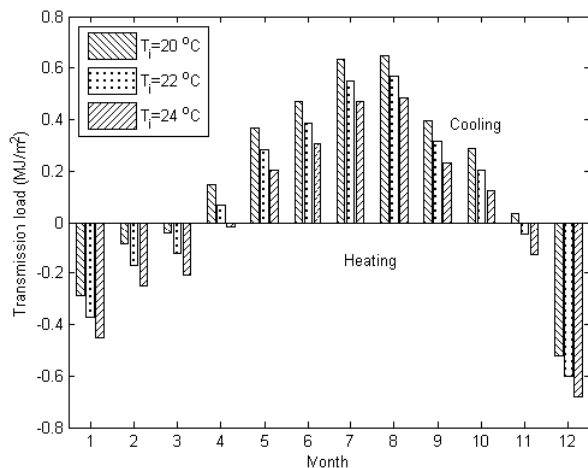


**(c)**

**Figure 6.** The daily total cooling and heating transmission loads for the 15th day of each month with respect to different indoor design temperatures in 6 cm insulated wall for (a) south, (b) north and (c) east (or west) orientations.

Table 4 shows yearly heating, yearly cooling and yearly total transmission loads according to indoor design temperatures for different wall orientations. The results indicate that minimum heating load is obtained in the south-facing wall while the minimum cooling load is obtained in the north-facing wall. The same conclusion was previously obtained for the climatic conditions of Elazığ, Turkey (Ozel, 2016). The results also indicate that as indoor design temperature rises, the cooling load and total load decrease while the heating load increases. It is obvious that total transmission load is reduced since the cooling load is more dominant than the heating load under the climatic conditions of Adana, Turkey. It is also obvious that the wall orientation, indoor design temperatures and insulation have a significant effect on heating, cooling and total transmission loads.

**Table 4.** The effect of indoor design temperatures on the yearly cooling, heating and total transmission loads for different wall orientations

| Indoor design temp. (°C) | Wall orientation | The yearly transmission loads (MJ/m² year) | | | | | |
|---|---|---|---|---|---|---|---|
| | | Uninsulated wall | | | Insulated wall | | |
| | | Heat. | Cool. | Total | Heat. | Cool. | Total |
| 20 | South | 73.5 | 359.7 | 433.2 | 18.6 | 91.0 | 109.6 |
| | North | 136.2 | 279.2 | 415.4 | 34.4 | 70.6 | 105.1 |
| | East/West | 112.0 | 361.9 | 473.9 | 28.3 | 91.5 | 119.9 |
| 22 | South | 111.3 | 279.8 | 391.1 | 28.2 | 70.8 | 98.9 |
| | North | 186.9 | 212.3 | 399.2 | 47.3 | 53.7 | 100.9 |
| | East/West | 156.4 | 288.6 | 445.0 | 39.6 | 73.0 | 112.6 |
| 24 | South | 154.7 | 205.6 | 360.3 | 39.1 | 52.0 | 91.1 |
| | North | 245.1 | 152.8 | 397.9 | 62.0 | 38.6 | 100.6 |
| | East/West | 206.6 | 221.2 | 427.7 | 52.3 | 55.9 | 108.2 |

Indoor design temperatures and the heating and cooling periods which are determined from the thermal performance point of view are given in Table 5 for each month's representative day according to wall orientations. These results indicate that for the south wall, yearly heating load is obtained during the heating period (December, January and February) while the yearly cooling load is obtained during the cooling period (from March to November). For a north-facing wall, the heating period consists of November, December, January, February, March and April months while the cooling period consists of May, June, July, August, September and October months. On the other hand, it is seen that for east (or west) orientations, the heating period consists of November, December, January, February and March months while the cooling period consists of April, May, June, July, August, September and October months. It is seen that the longest cooling period is obtained in south orientation while the shortest cooling period is obtained in north orientation. It is also seen that the shortest heating period is obtained in south orientation.

**Table 5.** The indoor design temperatures and the heating and cooling periods which are determined for the representative day of each month according to different wall orientations

| Orientation | Indoor design temperatures $T_i$(°C) | | | | | | | | | | | |
|---|---|---|---|---|---|---|---|---|---|---|---|---|
| | Jan | Feb | Mar | Apr | May | Jun | Jul | Aug | Sep | Oct | Nov | Dec |
| South | 20[h] | 20[h] | 20[c] | 22[c] | 24[c] | 24[c] | 24[c] | 24[c] | 24[c] | 22[c] | 20[h] | 20[h] |
| North | 20[h] | 20[h] | 20[h] | 22[h] | 24[c] | 24[c] | 24[c] | 24[c] | 24[c] | 24[c] | 22[h] | 20[h] |
| East/West | 20[h] | 20[h] | 20[h] | 22[c] | 24[c] | 24[c] | 24[c] | 24[c] | 24[c] | 24[c] | 22[h] | 20[h] |

[h]heating
[c]cooling

## Determination of Daily and Yearly Transmission Loads

Fig. 7 presents variation of daily total cooling and heating transmission loads according to months for different wall orientations in 6 cm insulated wall. These transmissions are determined by using the interior design temperatures given in Table 5. It is revealed that the minimum heating load is obtained in February for the south-facing wall while the maximum heating load is obtained in December for the north-facing wall.
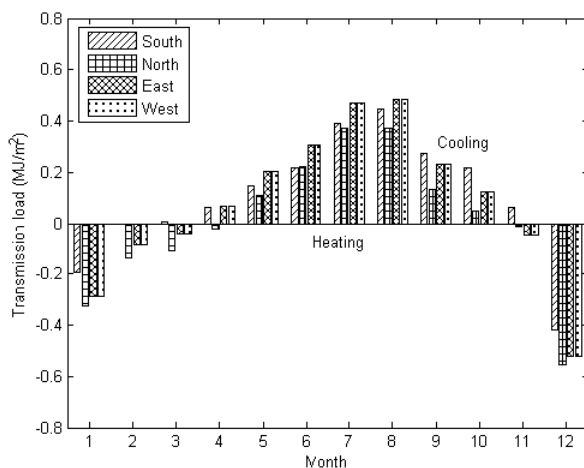


**Figure 7.** The daily total cooling and heating transmission loads for the 15th day of each month with respect to different wall orientations in 6 cm insulated wall

Fig. 8 indicates yearly cooling and heating loads to insulation thicknesses for different wall orientations. The yearly total transmission load is also shown in Fig. 9. It is seen that in the uninsulated wall, yearly cooling load is obtained to be 221.37, 152.81, 229.14 and 229.14 MJ/m² for the south, north, east and west orientations, respectively while yearly heating load is obtained to be 73.54, 138.44, 117.62 and 117.62 MJ/m². The results show that the cooling load is greater than the heating load. Besides, it is obvious that all transmission loads decrease against increased insulation thickness. This reduction is greater in the smaller insulation thickness values. With the increase of the insulation thickness, the transmission loads approach each other for all wall orientations. It is seen that in 10 cm insulated wall, yearly cooling load is obtained to be 37.37, 25.79, 38.68 and 38.68 MJ/m² for south, north, east and west orientations, respectively while yearly

heating load is obtained to be 12.41, 23.36, 19.85 and 19.85 MJ/m². The results show that the amount of reduction in heating, cooling and total loads is 83.12% for all wall orientations when the wall is insulated as 10 cm. The results also show that the transmission loads are the same for east and west orientations. The other orientations have almost equal cooling loads while the north-facing wall gives the lowest cooling load. It is obvious that inside surface temperature swings and peak loads as seen in Fig.4 are different for south, north, east and west orientations because of solar radiation. However, these loads are obtained as equal for the east and west orientations since yearly transmission loads are calculated from the sum of the instant loads. This is because the incident solar radiation is symmetrical for the east and west orientations, and these orientations receive the same amount of total solar radiation. The north-facing wall gives maximum heating load while the south-facing wall gives minimum heating load. Same trends and similar results were achieved by references (Ozel, 2011; Al-Sanea and Zedan, 2002; Daouas, 2011) for different climates. At lower insulation thicknesses, the total transmission load of the north-facing wall is slightly smaller than that of the south-facing wall. With the increase of the insulation thickness, total transmission loads of south and north-facing walls begin to be the same. The highest values of total transmission load are obtained in east and west-facing walls as obtained in cooling load.
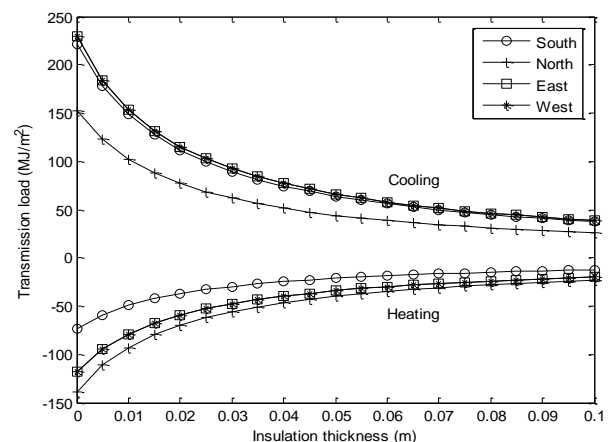


**Figure 8.** Variation of yearly cooling and heating transmission loads versus insulation thickness for different wall orientations
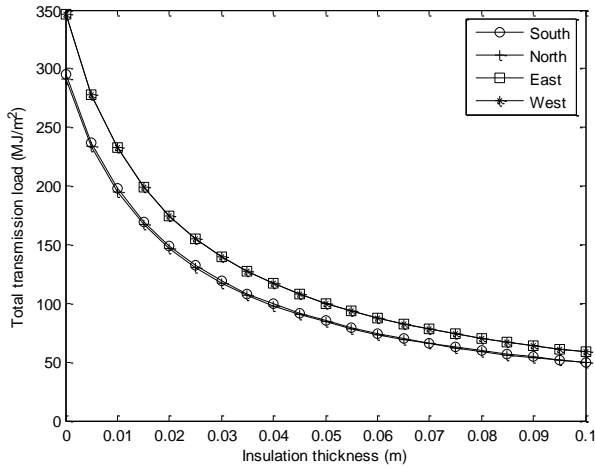
**Figure 9.** Variation of yearly total transmission loads versus insulation thickness for different wall orientations.

**Determination of Dynamic Thermal Resistance**

Fig. 10 (a-b) demonstrates the variation of thermal resistance values versus the 15th day of each month according to different wall orientations for uninsulated and insulated walls, respectively. Fig. 10 also demonstrates nominal resistance (Rn) to compare with dynamic resistance. The static resistance does not vary according to the wall orientations as it does not include the effects of solar radiation and heat storage. Besides, it has the same value for all months since the static resistance is the sum of conductive and convective resistances. It is seen that the static resistance is obtained to be 0.5347 $m^2$K/W in the uninsulated wall for all months while it is obtained to be 2.1136 $m^2$K/W in the insulated wall. The results show that the dynamic resistance varies according to the wall orientations and months. It is seen that the static resistance is greater than the dynamic resistance for all wall orientations in January, May, June, July, August, September months while it is smaller than the dynamic resistance in November, December, February, March and April months. It is also seen that dynamic and static thermal resistances increase when the wall is insulated.

The dynamic thermal resistance values of uninsulated and insulated walls are compared in Fig. 11 (a-d). It is seen that peak resistance values in some months of the year are obtained if the wall is insulated. For example, when the wall is 6 cm insulated, the maximum peak value of dynamic resistance is obtained in February for the south-facing wall, in April for the north-facing wall and in March for the east (or west)-facing walls because of minimum heating loads. These months correspond to months of minimum heating as shown in Fig. 7. The results show that dynamic thermal resistance is minimum in months that heating and cooling loads are maximum. It is seen that for south orientation and February month, dynamic thermal resistance is obtained to be 9.1234 $m^2$K/W in the insulated wall while it is obtained to be 0.9511 $m^2$K/W in the uninsulated wall.
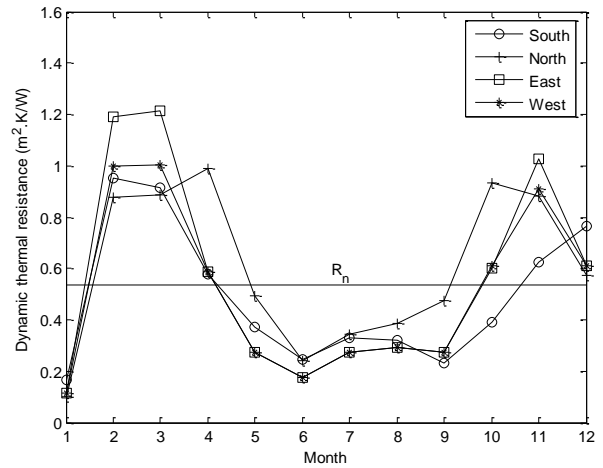


**(a)**
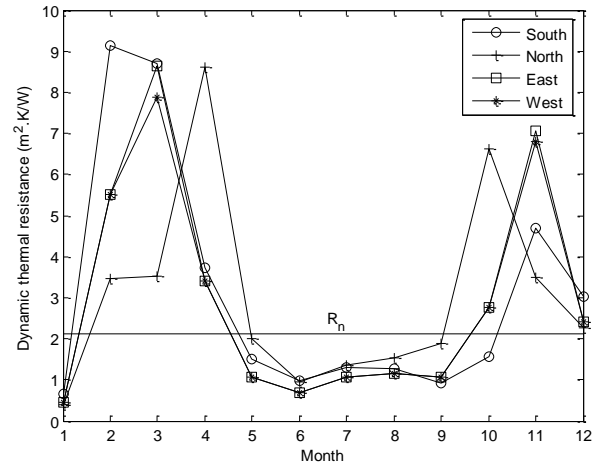


**(b)**

**Figure 10.** Variation of thermal resistance values versus months according to different wall orientations for a) uninsulated wall and b) 6 cm insulated wall.

Fig. 12 shows the variation of thermal resistance values versus insulation thickness according to all months for the south-facing wall. It is seen that the static resistance is higher than the dynamic resistance for some months of the year. It is also seen that the dynamic resistances for all months and nominal resistance linearly increase with the increase of insulation thickness. The results demonstrate that the gradient of the resistance versus insulation thickness is different for each month. It is seen that for the south-facing wall, the gradient of the resistance is maximum in February month while it is minimum in January month.

**(a)**



**(b)**



**(c)**



**(d)**
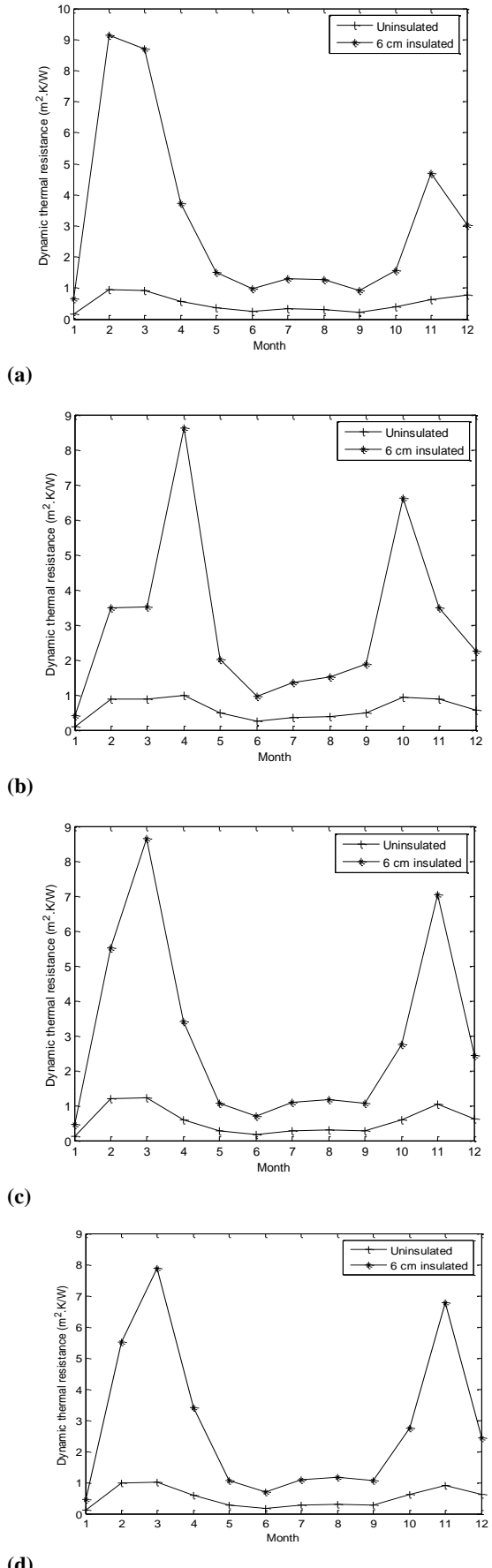
**Figure 11.** Variation of dynamic thermal resistance versus months according to uninsulated and insulated walls for a) south b) north c) east and d) west orientations
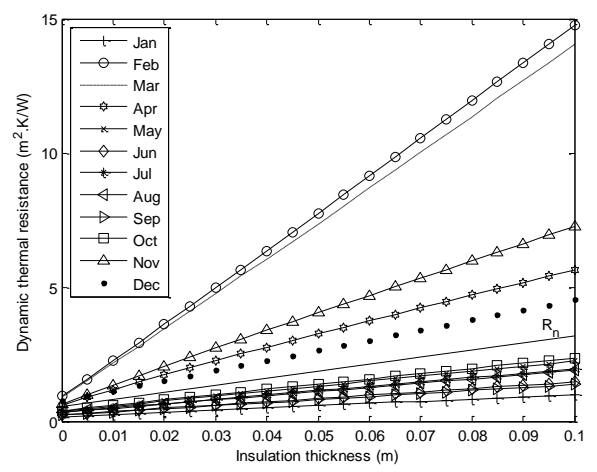


**Figure 12.** Variation of thermal resistance values versus insulation thickness according to all months for south-facing wall.

Fig. 13 shows the variation of annual averaged dynamic thermal resistance to increasing insulation thickness for different wall orientations. The dynamic resistance differs according to wall orientations since it contains the effects of heat storage and solar radiation. It is seen that in 6 cm insulated wall, the dynamic resistance values are obtained to be 1.956, 1.937, 1.708 and 1.705 $m^2$K/W while in the uninsulated wall, they are obtained to be 0.480, 0.446, 0.412 and 0.406 $m^2$K/W for the north, south, east and west orientations, respectively. The results demonstrate that the highest dynamic resistance is obtained in the north-facing wall then the south-facing wall while the lowest dynamic resistance is obtained in east and west-facing walls.
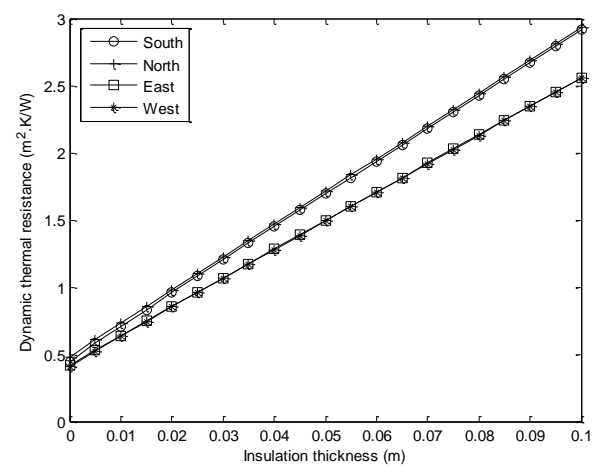


**Figure 13.** Variation of dynamic thermal resistance versus insulation thickness for different wall orientations

**Determination of Time Lag and Decrement Factor**

Fig. 14 (a-b) shows the time lag and decrement factor for the 15th day of each month according to different wall orientations. It is revealed that for all months, maximum time lag appears in the east wall while minimum time lag appears in the west wall. Besides, it is seen that the minimum decrement factor is obtained

in the west-facing wall for January, February, March, October, November and December months while it is obtained in the east-facing wall for April, May, June, July, August and September months.
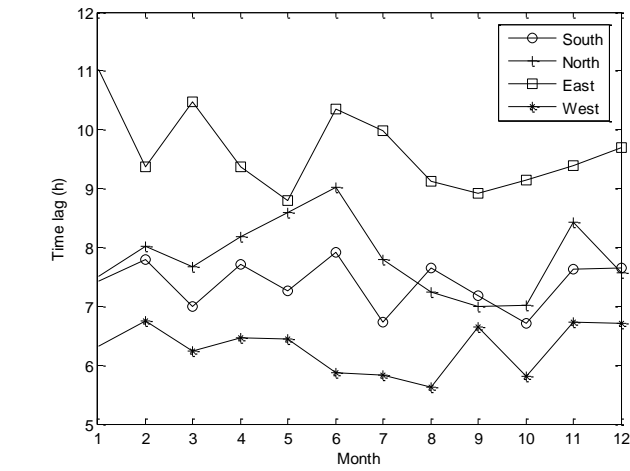


**(a)**
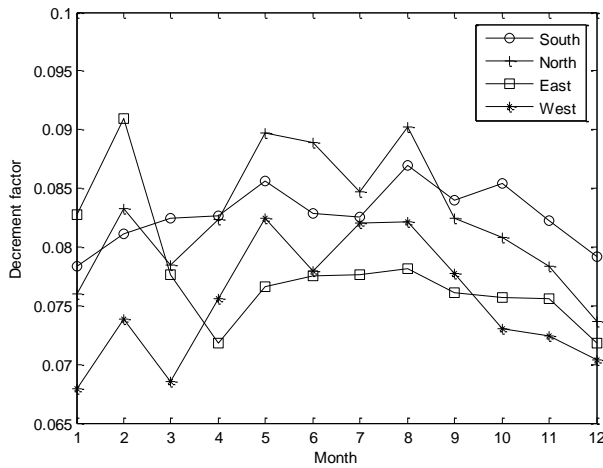


**(b)**

**Figure 14 (a-b).** Variation of time lag and decrement factor for the 15th day of each month according to different wall orientations

Fig. 15 (a-b) presents the variation of time lag and decrement factor according to increasing insulation thickness for wall orientations. The results indicate that as insulation thickness rises, time lag increase for whole wall orientations while the decrement factor decreases, as expected. The east-oriented wall gives maximum time lag while west oriented wall gives minimum time lag. This is because the maximum peak value of outside surface temperature reaches earlier for the east-facing wall and reaches later for the west-facing wall as seen in Fig.3. However, it is seen that at the lower thickness of insulation, the west-facing wall gives a slightly lower decrement factor than the other orientations. As the thickness of insulation rises, decrement factors for all wall orientations approach each other. Similar conclusions were obtained for different insulation materials under different climatic conditions (Al-Sanea and Zedan 2002). The best result from the maximum time lag point of view is achieved in the east-facing wall

while the worst result from the minimum time lag point of view is obtained in the west-facing wall. The conclusions of this study are consistent with those obtained by employing different climate conditions (Ozel 2013a; Ozel 2013b; Ramin, et al. 2016; Al-Sanea and Zedan 2002).
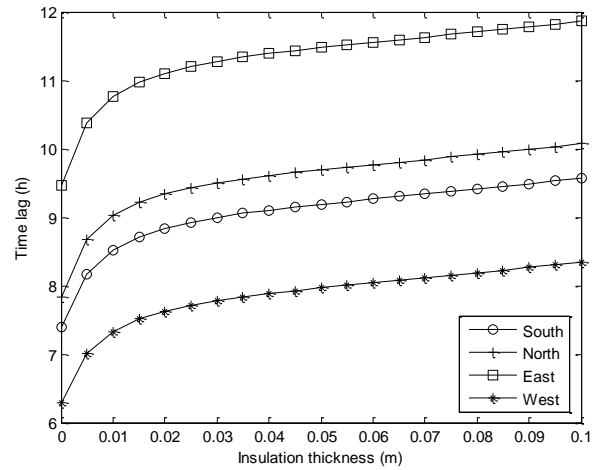


**(a)**
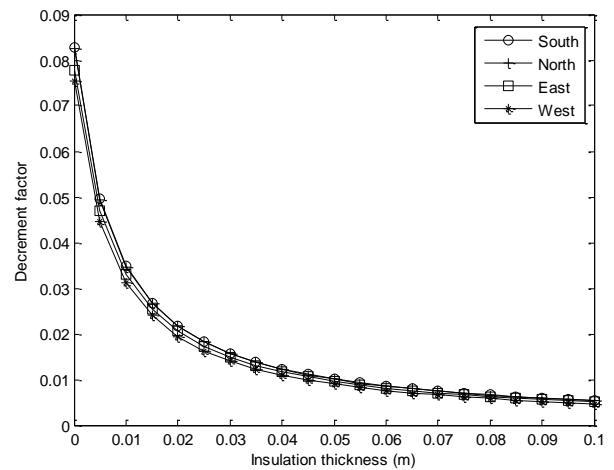


**(b)**

**Figure 15 (a-b).** Variations of time lag and decrement factor with insulation thickness for different wall orientations.

Change of time lag and decrement factor according to different orientations for uninsulated and insulated walls is presented in Fig. 16 (a-b). For uninsulated walls, the time lag is obtained to be 7.39, 7.84, 9.47 and 6.29 h for the same orientations while the decrement factor is obtained to be 0.0828, 0.0824, 0.0777 and 0.0753 for the south, north, east and west orientations, respectively. The results indicate that the wall orientation has a very small effect on the decrement factor, but has a large effect on the time lag. The results also indicate that the decrement factor is reduced while the time lag rises if the wall is insulated. For 6 cm insulation thickness, it is seen that this increase in time lag is 25.4%, 10.95%, 22.01% and 27.83% while this reduction in decrement factor is 89.61%, 89.68%, 89.58% and 89.91% for the south, north, east and west orientations, respectively.

The results show that the effect of insulation on the decrement factor is greater than its effect on time lag.



**(a)**



**(b)**
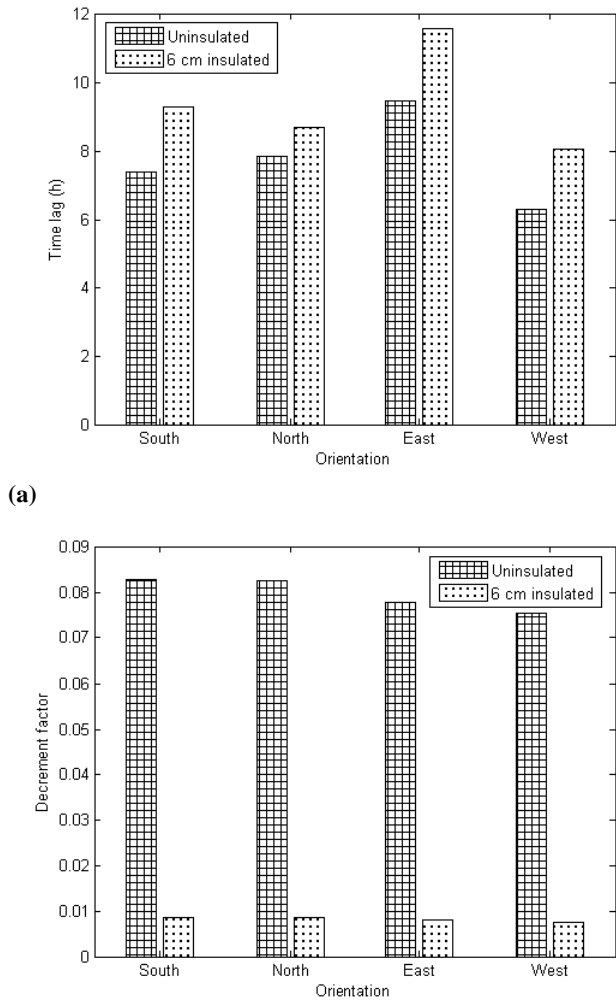
**Figure 16 (a-b).** Variation of time lag and decrement factor according to different wall orientations

**Determination of Optimum Insulation Thickness**

Fig. 17 indicates the variation of costs versus increased insulation thickness for the south-facing wall. It is seen that with increasing the insulation thickness, the cost of the insulation rises linearly while the cost of the energy decreases. It is also seen that the total cost which consists of the cost of energy and insulation diminishes up to a certain value of insulation thickness and then started to increase. The variation of total cost according to increasing insulation thickness for all wall orientations is shown in Fig. 18. The optimum insulation thickness is insulation thickness where the total cost is the minimum. The conclusions indicate that the optimum thickness of the insulation is obtained to be 8.4 cm for the south, 8.0 cm for north, 9.2 cm for east and west orientations, respectively. The results of the present study on the optimum insulation thickness according to the different wall orientations are compared with the results of other studies in Table 6. It is obvious that optimum insulation thicknesses of east

and west-facing walls which have the same yearly heating and cooling loads are the same. The results illustrate that for some climatic conditions, the lowest insulation thickness is achieved on the north-facing wall while for other climatic conditions, it is achieved on the south-facing wall. However, it is seen that for most climates, east and west orientations give the greatest insulation thickness. In warm climates such as Adana, it is clear that the minimum insulation thickness is achieved for the north wall. In this study, it is seen that the north orientation provides the lowest insulation thickness while east (or west) orientation provides the highest insulation thickness.
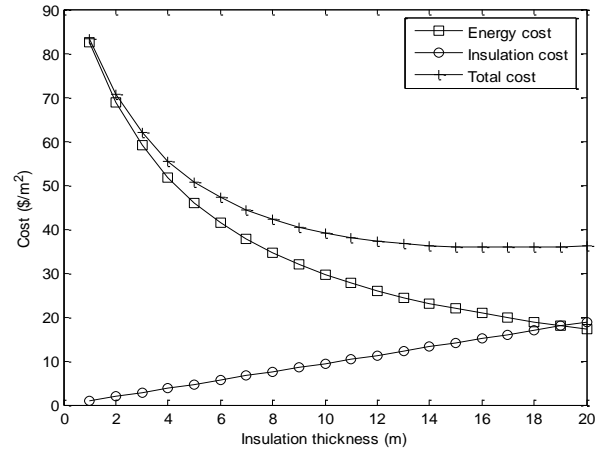


**Figure 17**. Variation of costs with insulation thickness for a south-facing wall.
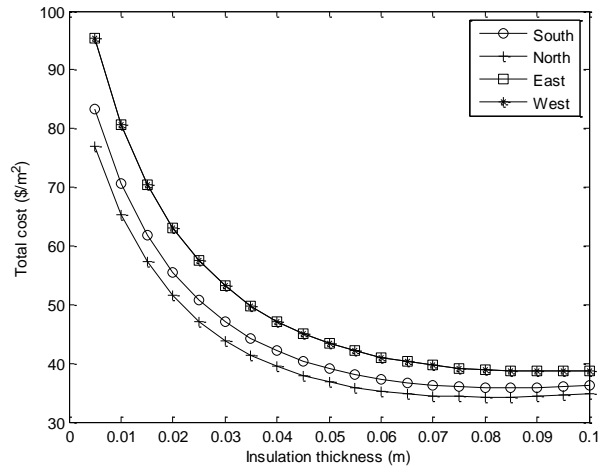


**Figure 18**. Variation of total cost with insulation thickness for different wall orientations.

**Table 6.** Comparison of the results of the present study with the results of other studies on the optimum insulation thickness according to the different wall orientations

| Reference study | Location | Insulation materials | Optimum insulation thickness (cm) | | | |
|---|---|---|---|---|---|---|
| | | | South | North | East | West |
| Present study (heating+cooling) | Adana, Turkey | Expanded polystyrene | 8.4 | 8.0 | 9.2 | 9.2 |
| Ozel, (2011) (heating+cooling) | Elazığ, Turkey | Extruded polystyrene | 5.5 | 6.0 | 6.0 | 6.0 |
| Ozel, (2013) (heating) | Kars, Turkey | Expanded polystyrene | 13.6 | 15.0 | 14.4 | 14.4 |
| | Kars, Turkey | Extruded polystyrene | 9.2 | 10.2 | 9.8 | 9.8 |
| Ozel, (2013) (cooling) | Antalya, Turkey | Extruded polystyrene | 3.6 | 3.1 | 4.0 | 4.0 |
| Nematchoua et. al. (2017) (cooling) | Yaounde, Cameroon | Expanded polystyrene | 8.0 | 7.0 | 8.0 | 8.0 |
| | Garoua, Cameroon | Expanded polystyrene | 12.0 | 11.0 | 12.5 | 12.5 |
| Huo et. al. (2015)(heating+cooling) | Chengdu, China | Expanded polystyrene | 6.1 | 6.1 | 6.2 | 6.2 |
| | Changsha, China | Expanded polystyrene | 7.3 | 7.5 | 7.7 | 7.7 |
| | Hefeie, China | Expanded polystyrene | 7.9 | 8.2 | 8.3 | 8.3 |
| | Shanghai, China | Expanded polystyrene | 6.8 | 7.2 | 7.2 | 7.2 |
| Ramin et. al. (2016) heating+cooling) | Tehran, Iran | Expanded polystyrene | 5.66 | 6.04 | 6.30 | 6.30 |
| | Tehran, Iran | Extruded polystyrene | 3.06 | 3.24 | 3.37 | 3.37 |
| Ibrahim et. al. (2012) (heating) | Zahle, Lebanon | Expanded polystyrene | 3.4 | 4.7 | 3.9 | 4.0 |
| Ibrahim et. al. (2012) (cooling) | Beirut, Lebanon | Expanded polystyrene | 4.1 | 1.9 | 4.8 | 4.9 |
| Al-Sanea and Zedan(2002)(heating+cooling) | Riyadh | Molded polystyrene | 8.75 | 8.88 | 9.2 | 9.25 |
| Daouas, (2011) (heating+cooling) | Tunisia | Expanded polystyrene | 10.10 | 10.1 | 11.7 | 11.6 |

## CONCLUSION

This study is realized for the climatic conditions of Adana which is one of the hottest cities of Turkey. Firstly, heating and cooling periods for different wall orientations are determined by calculating the transmission loads according to indoor design temperatures under dynamic thermal conditions. It is seen that for a south-facing wall, the heating period consists of December, January and February months while the cooling period consists from March to November. For a north-facing wall, the heating period consists from November to April while the cooling period consists from May to October. On the other hand, it is seen that for east (or west) orientations, the heating period consists from November to March while the cooling period consists from April to October. The results show that the longest cooling period is obtained in south orientation while the shortest cooling period is obtained in north orientation. The results also show that the wall orientation has an important effect on heating and cooling periods.

Secondly, thermal parameters such as transmission loads, dynamic thermal resistance, time lag and decrement factor are calculated for all wall orientations by using indoor design temperatures determined over the whole year. The results show that the other orientations have almost equal cooling loads while the minimum cooling load is obtained for the north-facing wall. Besides, it is seen that maximum heating load is obtained in the north wall while the minimum heating load is obtained in the south wall.

It is revealed that the dynamic resistance is inversely proportional to the total transmission load. That is, the maximum thermal resistance corresponds to the minimum transmission load. The results show that the north-facing wall then the south-facing wall give the lowest yearly total transmission load, the lowest insulation thickness and the highest dynamic thermal resistance. On the other hand, west and east-facing walls give the highest yearly total transmission load, the highest insulation thickness and the lowest dynamic thermal resistance.

Besides, the results show that the east-facing wall has the longest time lag since the maximum value of the outer surface temperature is reached at the earliest east wall. It is seen that the effect of the wall orientation on the decrement factor is unimportant while the wall orientation has an important effect on time lag. Finally, the optimum thickness of insulation is determined by using both heating and cooling loads. The results obtained for different wall orientations are compared with the results of other studies under different climatic conditions.

Consequently, it is seen that wall orientation has a noticeable effect on time lag, dynamic thermal resistance, transmission loads and optimum insulation thickness while the effect of wall orientation on decrement factor and static thermal resistance are insignificant.

## REFERENCES

Akan A. E., 2021, Determination and Modeling of Optimum Insulation Thickness for Thermal Insulation of Buildings in All-City Centers of Turkey, *International Journal of Thermophysics,* 42, 49, 1-34.

Aktemur C., Bilgin F. and Tunçkol S., 2021, Optimization on the Thermal Insulation Layer Thickness in Buildings with Environmental Analysis: an Updated Comprehensive Study for Turkey's all Provinces, *Journal of Thermal Engineering*, 7, 5, 1239–1256.

Al-Sanea S.A., Zedan M. F., and Al-Ajlan S. A., 2003, Heat Transfer Characteristics and Optimum Insulation Thickness for Cavity Walls, *Journal of Thermal Envelope and Building Science,* 26, 3, 285-307.

Al-Sanea S.A., and Zedan M. F., 2002, Optimum Insulation Thickness for Building Walls in a Hot-Dry Climate, *International Journal of Ambient Energy,* 23, 3, 115-126.

Al-Sanea S.A., Zedan M. F. and Al-Hussain S. N., 2013, Effect of Masonry Material and Surface Absorptivity on Critical Thermal Mass in Insulated Building Walls, *Applied Energy*, 102, 1063-1070.

Al-Sanea S.A., Zedan M. F. and Al-Ajlan, S. A., 2005, Effect of Electricity Tariff on The Optimum Insulation-Thickness in Building Walls as Determined by a Dynamic Heat-Transfer Model, *Applied Energy,* 82, 313-330.

Barrau J., Ibanez M. and Badia F., 2014, Impact of the İnsulation Materials' Features on The Determination of Optimum Insulation Thickness, *International Journal of Energy and Environmental Engineering*, 5, 2-3, 1-9.

Bolattürk A., 2008, Optimum Insulation Thicknesses For Building Walls with Respect to Cooling and Heating Degree-Hours in the Warmest Zone of Turkey, *Building and Environment,* 43, 1055-1064.

Bolattürk A., 2006, Determination of Optimum Insulation Thickness for Building Walls with respect to Various Fuels and Climate Zones in Turkey, *Applied Thermal Engineering*, 26, 1301-1309.

Çomaklı K. and Yüksel B., 2003, Optimum Insulation Thickness of External Walls for Energy Saving, *Applied Thermal Engineering*, 23, 473-479.

Çomaklı K. and Yüksel B., 2004, Environmental Impact of Thermal Insulation Thickness in Buildings, *Applied Thermal Engineering*, 24, 933-940.

Daouas N., Hassen Z. and Aissia H. B., 2010, Analytical Periodic Solution for The Study of Thermal Performance and Optimum Insulation Thickness of Building Walls in Tunisia, *Applied Thermal Engineering*, 30, 319-326.

Daouas N., 2011, A Study on Optimum Insulation Thickness i Walls and Energy Savings in Tunisian Buildings based on Analytical Calculation of Cooling and Heating Transmission Loads, *Applied Energy,* 88, 156-164.

Dombaycı Ö. A., Gölcü M. and Pancar Y., 2006, Optimization of Insulation Thickness for External Walls for Different Energy-Sources, *Applied Energy,* 83, 9, 921-928.

Dombaycı Ö. A., 2007, The Environmental Impact of Optimum Insulation Thickness for External Walls of Buildings, *Energy and Buildings*, 42, 3855-3859.

Dombaycı Ö. A., Atalay Ö., Acar S. G., Ulu E. Y. and Ozturk H. K., 2017, Thermoeconomic Method for Determination of Optimum Insulation Thickness of External Walls for The Houses: Case Study for Turkey, *Sustainable Energy Technologies and Assessments,* 22, 1–8.

Duffie J. A., & Beckman W. A., 1991, Solar Engineering Of Thermal Processes, John Wiley and Sons, inc., New York.

Ertürk M., 2016, A New Approach to Calculate The Energy Saving Per Unit Area and Emission Per Person in Exterıor Wall of Building using Different Insulation Materıals and Air Gap, *Journal of the Faculty of Engineering and Architecture of Gazi University*, 31(2), 395-406.

Ertürk M., 2017, A New Model for Exergetic Optimum Insulation Thickness, *International Journal of Exergy*, 22, 3, 309-330.

Hasan A., 1999, Optimizing Insulation Thickness for Buildings using Life Cycle Cost, *Applied Energy,* 63, 115-124.

Huo H., Jing C. and Huo H., 2015, Effect of Natural Ventilation on Transmission Load of Building External Walls and Optimization of Insulation Thickness, *Journal of thermal science and technology*, 10, 2, 1-17.

Ibrahim M., Ghaddar N. and Ghali K., 2012, Optimum Location And Thickness of Insulation Layers for Minimizing Building Energy Consumption, *Journal of Building Performance Simulation*, 5, 6, 384-398.

Kaynakli O., 2008, A Study on Residential Heating Energy Requirement and Optimum Insulation Thickness, *Renewable Energy*, 33, 1164-1172.

Kaynaklı O., Yüce C., Dogan O., and Kaynaklı Z., 2015, A Study on Determınatıon of Optımum Thermal Insulatıon Thıckness usıng Life Cycle Cost Analysis, *International Journal of Advances in Mechanical and Civil Engineering*, 2, 6, 1-5.

Kontoleon K. J., Theodosiou ThG. and Tsikaloudaki K. G., 2013, The Influence of Concrete Density and Conductivity on Walls' Thermal Inertia Parameters Under a Variety of Masonry and Insulation Placements, *Applied Energy,* 112, 325–337.

Kurt H., 2010, The Usage of Air Gap in The Composite Wall for Energy Saving and Air Pollution, Environmental Progress and Sustainable Energy 30, 450-458.

Mahlia T. M. I. and Iqbal A., 2010, Cost Benefits Analysis and Emission Reductions of Optimum Thickness and Air Gaps for Selected Insulation Materials for Building Walls Maldives, *Energy*, 35, 2242-2250.

Nematchoua M. K., Ricciardi P., Reiter S., and Yvon A., 2017, A Comparative Study on Optimum Insulation Thickness of Walls and Energy Savings in Equatorial and Tropical Climate, *International Journal of Sustainable Built Environment,* 6, 170-182.

Ozel M., 2011, Effect of Wall Orientation on The Optimum Insulation Thickness by Using a Dynamic Method, *Applied Energy,* 88, 2429-2435.

Ozel M., 2013a, Thermal, Economical and Environmental Analysis of Insulated Building Walls in a Cold Climate. *Energy Conversion and Management,* 76, 674-684.

Ozel M., 2013b, Determination of Optimum Insulation Thickness Based on Cooling Transmission Load for Building Walls in a Hot Climate, *Energy Conversion and Management*, 66, 106-114.

Ozel, M., & Pihtili, K. (2007). Optimum Location and Distribution of Insulation Layers on Building Walls with Various Orientations. *Building and Environment,* 42, 3051-3059.

Ozel, M. (2016).  Effect of Indoor Design Temperature on The Heating and Cooling Transmission Loads. *Journal of Building Engineering*, 7, 46–52.

Ozkahraman H. T. and Bolattürk A., 2006, The Use of Tuff Stone Cladding in Buildings for Energy Conservation, *Construction and Building Materials*, 20, 435-440.

Özel G., Açıkkalp E., Görgün B., Yamık H. and Caner N., 2015, Optimum Insulation Thickness Determination Using The Environmental and Life Cycle Cost Analyses based Entransy Approach, *Sustainable Energy Technologies and Assessments,* 11, 87–91.

Ramin H., Hanafizadeh P. and Akhavan-Behabadi M. A., 2016, Determination of Optimum Insulation Thickness in Different Wall Orientations and Locations in Iran, *Advances in Building Energy Research*, 10, s2, 149-171.

Sisman N., Kahya E., Aras N. and Aras H., 2007, Determination of Optimum Insulation Thicknesses of The External Walls and Roof (Ceiling) for Turkey's Different Degree-Day Regions, *Energy Policy*, 35, 5151-5155.

State Meteorological Station, Records for weather data, Turkey, 2007-2017.

Sundarama, A. S. and Bhaskaran A., 2014, Optimum Insulation Thickness of Walls for Energy-Saving in Hot Regions of India, *International Journal of Sustainable Energy,* 33, 1, 213–226.

Threlkeld J. L., 1998, Thermal environmental engineering. Englewood Cliffs,NJ: Prentice-Hall.

Yıldız A., Gürlek G., Erkek M. and Özbalta N., 2008, Economical and Environmental Analyses of Thermal Insulation Thickness in Buildings, *Journal of Thermal Science and technology*, 28, 2, 25-34.

Yu J., Yang C., Tian L. and Liao D., 2009, A Study on Optimum Insulation Thicknesses of External Walls in Hot Summer and Cold Winter Zone of China, *Applied Energy,* 86, 2520-2529.

Zenginis D. G. and Kontoleon K. J., 2018, Influence of Orientation, Glazing Proportion and Zone Aspect Ratio on The Thermal Performance of Buildings During The Winter Period, *Environmental Science and Pollution Research,* 25, 27, 26736-26746.

**Meral ÖZEL** graduated from Department of Mechanical Engineering of Fırat University in 1992. She received his M.Sc. and Ph.D. degrees in Mechanical Engineering from Fırat University in 1996 and 2003, respectively. She became Associate Professor in 2014 and Professor in 2021. Currently, she is working as a faculty member at the same university.